Coronal mass ejection geoeffectiveness depending on field orientation and interplanetary coronal mass ejection classification

Seung-Mi Kang,[1,2] Y.-J. Moon,[3] K.-S. Cho,[3] Yeon-Han Kim,[3] Y. D. Park,[3] Ji-Hye Baek,[3] and Heon-Young Chang[1]

Received 31 December 2005; revised 11 January 2006; accepted 12 January 2006; published 26 May 2006.

[1] In this study, we have examined the coronal mass ejection (CME) geoeffectiveness characterized by Dst ≤ -50 nT according to the field orientation (N or S) in a CME source region and its dependence on interplanetary CME (ICME) classification (magnetic clouds or ejecta). We first considered 133 CME-ICME pairs (1996 to 2001) whose CME source locations are identified by SOHO Large-Angle Spectrometric Coronograph (SOHO/LASCO) and extreme ultraviolet imaging telescope (SOHO/EIT) data. Then we identified the shapes (S or Inverse-S) of the X-ray sigmoids associated with 63 of these CMEs using Yohkoh/Soft X-Ray Telescope (SXT) data. To determine the field orientation in the sigmoids, we applied the coronal flux rope (CFR) model and the force-free field (FFF) model to these 63 sigmoids using SOHO/Michelson Doppler Imager (MDI) images. We present the results in contingency tables, classified according to solar field orientation and geomagnetic storm strength/occurrence. We found that (1) the prediction of geomagnetic storms (Dst ≤ -50 nT) based on the CFR model is much better than that on the FFF model, (2) the prediction for magnetic clouds (MCs) is much better than that for ejecta (EJ), which implies that the field orientation of the MCs is well conserved through the heliosphere, and (3) for about 86% of the magnetic clouds, the directions of their leading fields are consistent with those in the CME source regions. Our results support the findings that the southward orientations of the magnetic field in the CME source regions plays an important role in the production of geomagnetic storms.

Citation: Kang, S.-M., Y.-J. Moon, K.-S. Cho, Y.-H. Kim, Y. D. Park, J.-H. Baek, and H.-Y. Chang (2006), Coronal mass ejection geoeffectiveness depending on field orientation and interplanetary coronal mass ejection classification, *J. Geophys. Res.*, *111*, A05102, doi:10.1029/2005JA011445.

1. Introduction

[2] It is well known that coronal mass ejections (CMEs) play an important role in producing geomagnetic storms, especially when there exist southward components of the interplanetary magnetic field (IMF) [*Zhang and Burlaga*, 1988; *Fenrich and Luhmann*, 1998]. One possible candidate for determining the southward orientation of the IMF preceding a geomagnetic storm is the field orientation in the CME source region. So far, the investigations of the solar origin of the southward component give results that are rather controversial [e.g., *Pevtsov and Canfield*, 2001; *Yurchyshyn et al.*, 2001; *Leamon et al.*, 2002]. *Pevtsov and Canfield* [2001] studied the relationship between the field orientations in the CME source region and the geomagnetic storms for 18 events. For the field orientation, they used two magnetic field models: a coronal flux rope (CFR) model and a force-free field (FFF) model. They found that when a CFR model was used to interpret magnetic structure, eruptions with southward leading magnetic fields were better associated with stronger geomagnetic storms while those with northward leading fields were less well associated with geomagnetic storms. *Yurchyshyn et al.* [2001] compared the magnetic field orientations in two eruptive active regions to the corresponding IMF orientations. To identify the orientations of magnetic fields in these eruptive regions, they adopted the linear force-free field model in order to compare model field lines with the overlying field lines deduced from Hα and/or EUV images. As a result, they found that the field orientation in eruptive filaments at the Sun were consistent with the direction of the axial field of flux ropes (magnetic cloud) at L1. Note that this linear force-free model is different from the FFF model by *Pevtsov and Canfield* [2001] in that while the first model is employed to show the direction of overlying fields, the

[1]Department of Astronomy and Atmospheric Sciences, Kyungpook National University, Daegu, South Korea.
[2]Also at Korea Astronomy and Space Science Institute, Daejon, South Korea.
[3]Korea Astronomy and Space Science Institute, Daejon, South Korea.

Copyright 2006 by the American Geophysical Union.
0148-0227/06/2005JA011445$09.00

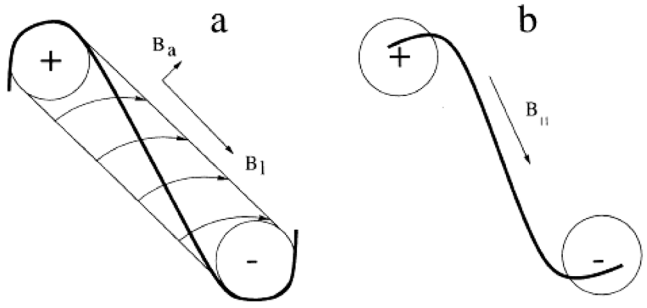

Figure 1. Field orientation of (a) the CFR and (b) the FFF model [*Pevtsov and Canfield*, 2001]. Circles indicate the positive and negative polarity. Thin lines connecting the two circles in Figure 1a indicate a flux rope projected onto the image plane. The field direction is left-handed when the flux rope is the inverse-S shape. When the left thumb indicates the direction from positive to negative polarity, the direction of the other fingers indicates the orientation of a flux rope. Similarly, the field direction is right-handed when the flux rope is the S sigmoidal shape. In the case of FFF model (Figure 1b), the orientation is opposite.

second one is used to indicate the field orientation in the X-ray sigmoid in an active region. On the other hand, *Leamon et al.* [2002] studied the association between the orientation predicted by the CFR model and the observed IMF Bz component of MC leading field. Their result showed that the correlation between the orientation predicted by CFR model and the observed IMF Bz component of magnetic cloud leading field was only 50% (nearly random) for the 46 solar eruption events compiled in several literatures.

[4] Interplanetary CMEs (ICMEs) can be mainly classified into two types: magnetic clouds (MCs) and ejecta (EJ). MCs are extensions of magnetic flux ropes into interplanetary space with strong magnetic fields, smooth north-south or south-north rotations of magnetic field, low IMF variations and low plasma beta [*Burlaga*, 1995]. EJ have similar characteristics to MCs, but do not show such smooth rotations. It is well known that there is a strong correlation between the Bz component of IMF and the Dst index [*Wu and Lepping*, 2002a, 2002b; *Yurchyshyn et al.*, 2003, 2004]. The magnetic field structures of MCs, such as smooth rotation patterns, may originate from flux-ropes in CME source regions [*Bothmer and Schwenn*, 1994; *Rust*, 1994;

[5] *McAllister and Martin*, 2000; *Yurchyshyn et al.*, 2001, 2003]. In the case of EJ, there has been no report on such a good correlation.

[6] The present paper is the third one of a series of papers on the investigation of CME geoeffectiveness. The first one [*Moon et al.*, 2005] suggested new geoeffective parameters (CME direction and column density) and found that there is a good correlation between these parameters and associated Dst values for very fast halo CMEs. The second one [*Kim et al.*, 2005] obtained the probability of CMEs being geoeffective by using the dependence of geomagnetic storm occurrence on CME speed and source location. In the present work, we examine the CME geoeffectiveness according to the field orientation in the CME source regions using 63 CME-ICME pairs from 1996 to 2001. We present the results in contingency tables, sorting the geomagnetic storm occurrence by CME/ICME field orientation. This work is a statistical extension of *Pevtsov and Canfield* [2001], who studied 18 events in 1991 to 1998. In addition, we study the effect of ICME classification on the geomagnetic storm prediction accuracy as well as on the relationship between the CME field orientation and the direction of ICME leading field. In section 2, we describe data selection and analysis. In section 3, we present observational results and discussions. A brief summary and conclusion are given in section 4.

2. Data and Analysis

2.1. Event Selection and Data Analysis

[7] We considered all CME-ICME pairs compiled from four papers described next. *Gopalswamy et al.* [2001] presented 47 CME-ICME pairs in 1996–2000 from SOHO and Wind spacecraft. They tabulated the location of a CME source region as well as its ICME classification (MCs/EJ) (refer to their Table 2). *Cane and Richardson* [2003] presented a comprehensive catalogue of 214 CME-ICME pairs in 1996–2002 from SOHO/LASCO and WIND data. *Cho et al.* [2003] gave the information on 38 solar disturbances (coronal shocks and CMEs) and their arrivals at L1 from 1997 to 2000. *Manoharan et al.* [2004] tabulated 91 interplanetary (IP) shocks associated with CMEs from 1997 to 2002. Regarding the location of a CME source region, we used the information given in the above references. When the information was not available, we determined the location of a CME source region directly by identifying temporal and spatial closeness between CMEs and coronal disturbances (e.g., flare brightening and/or EUV dimming) from SOHO/EIT, SOHO/LASCO, and GOES flare data. We selected events whose solar surface locations are identified and for which SXT data are available. As a result, we obtained 133 CME-ICME pairs. Finally, we identified noticeable sigmoids for 63 events.

[8] There are two different magnetic field models which identify the orientation of magnetic field in an active region: the coronal flux rope (CFR) model and the force-free field (FFF) model. In the CFR model, the magnetic field in the active region incorporates a helical structure like that of flux ropes seen in interplanetary clouds [*Gosling*, 1990; *Bothmer and Rust*, 1997]. The projected magnetic separatrix surface has a sigmoidal shape: S-shape when the flux rope is right-handed and inverse S-shape when it is left-handed

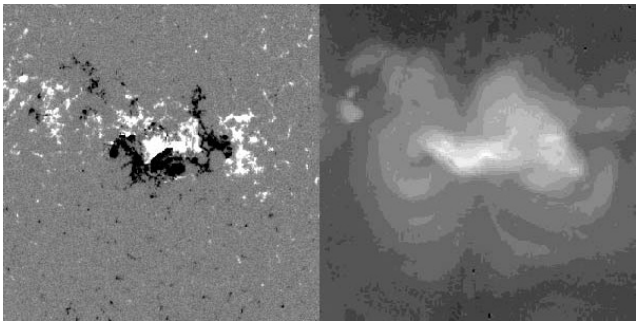

Figure 2. (left) SOHO/MDI and (right) Yohkoh/SXT images for the Bastille day event that occurred at 1054 UT on 14 July 2000. In the MDI image, the black area indicates the negative polarity and the white area indicates the positive polarity. The right image shows an inverse S sigmoidal shape in Yohkoh/SXT image. Note that the direction of the thumb is leftward since the left ending point of the sigmoid is evidently located on the negative sunspot. According to the left-handed rule, the field orientation based on the CFR model is southward (downward).

(Figure 1a). In the FFF model [*Pevtsov and Canfield*, 2001], the projected field lines in the core of active region correspond to sigmoidal shape (Figure 1b). We applied these two magnetic field models (CFR and FFF) to these X-ray sigmoids to determine the orientation of magnetic fields in the CME source regions using SOHO/MDI images. Figure 2 shows an example of SOHO/MDI and Yohkoh SXT images for Active Region AR 9077 in which the Bastille day event (14 July 2000 1054 UT) occurred. The SXT image shows the inverse-S shape sigmoid. Since the field direction is left-handed when the flux rope is the inverse-S shape (for details, see Figure 1), the orientation of the magnetic field is determined to be southward. In the case of FFF model, the orientation is opposite (northward). In similar ways, we could determine the orientation of the 63 events.

[9] The identification of MCs or EJ was taken from *Gopalswamy et al.* [2001], *Cho et al.* [2003], *Cane and Richardson* [2003], *Baek et al.* [2005], and the MC web page (http://lepmfi.gsfc.nasa.gov/mfi/mag_cloud_pub1.html). When the information is not available, we directly determined MC or EJ according to the conventional criteria [*Burlaga*, 1995] described in the previous section. To determine the geomagnetic storms (characterized by Dst index) associated with the ICMEs, we used the information given by *Cane and Richardson* [2003]. Otherwise, we determined the Dst value as a local minimum within ±1- day window from the ICME starting time using OMNIWEB data (http://nssdc.gsfc.nasa.gov/omniweb/form/dx1.html). The direction of MC leading field is defined as that of Bz component in the leading part of sinusoidal IMF variation, which is expected to correspond to the first part of the magnetic field in a flux rope. Figure 3 shows the IMF and Dst index for the Bastille day event. In the IMF Bz component, we can see a clear rotation of field direction from south to north. In this case, the direction of MC leading field is south. We note that there is a very strong geomagnetic storm having about −300 nT just after the minimum value of IMF southward Bz component.

2.2. Statistical Methodology

[10] For statistical evaluation of the consistency between solar field orientation and geomagnetic storm, we used a contingency table that has been widely used in weather forecast as well as in space weather research [e.g., *Smith et al.*, 2000; *Fry et al.*, 2003; *Kim et al.*, 2005]. Parameters (H, F, M, C) used in the contingency table and statistical verification parameters (PODy, PODn, FAR, CSI) are explained in Table 1. In this study, we assume that if the orientation of magnetic field in a CME source region is southward, then "Prediction" is "Yes"; otherwise (northward), prediction is "No." "Observation" is assumed to be

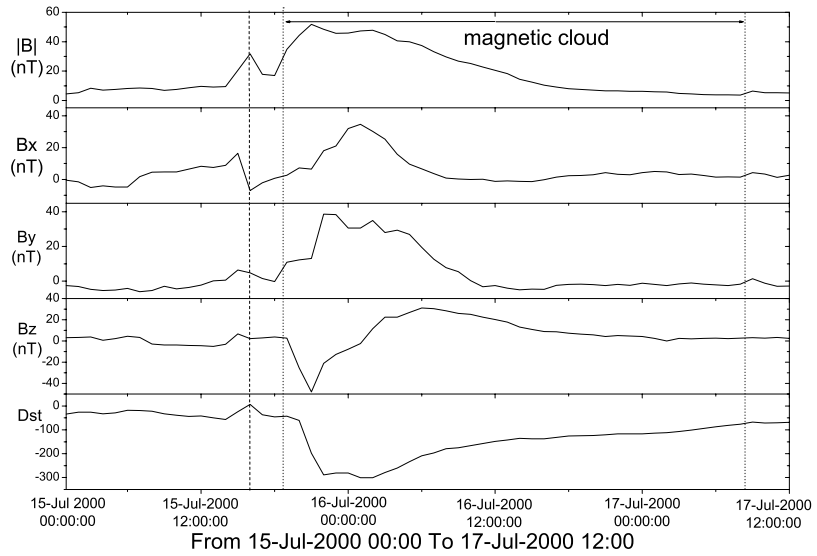

Figure 3. Variations of IMF and Dst index associated with the Bastille day event. This event was associated with a MC. The dotted lines indicate the start and end times of the MC. The dashed line is the starting time of an associated IP shock.

Table 1. Statistical Verification Parameters[a]

Statistic	Abbreviation	Definition
Probability of detection, yes	PODy	$H^b/(H + M^c)$, proportion of Yes observations that were correctly forecast
Probability of detection, no	PODn	$C^d/(F^e + C)$, proportion of No observations that were correctly forecast
False alarm ratio	FAR	F/(H + F), proportion of Yes forecasts that were incorrect
Critical success index	CSI	H/(H + F + M), proportion of hits that were either forecast or observed

[a]From *Smith et al.* [2000].
[b]Hit: the prediction is "Yes" and the observation is "Yes."
[c]Miss: the prediction is "No" but the observation is "Yes."
[d]Correct null: the prediction is "No" and the observation also is "No."
[e]False alarm: the prediction is "Yes" but the observation is "No."

"Yes" for $Dst \leq -50$ nT (geomagnetic storm) and "No" for $Dst > -50$ nT (nongeomagnetic storm). Usually, a high value of PODy, PODn, or CSI and a low value of FAR imply a good prediction. The perfect prediction is characterized by PODy = 1, PODn = 1, CSI = 1, and FAR = 0. On the other hand, the random prediction gives that PODy = 0.5, PODn = 0.5, CSI = 0.33, and FAR = 0.5.

3. Results and Discussion

[11] Table 2 summarizes the information of the 63 events whose sigmoidal shapes are clearly identified. It includes the Active Region number, the erupting time, the location of a CME source region, the sigmoidal shape (S or inverse-S), the orientation of magnetic field in the CME source region, the ICME classification (MCs or EJ), the direction of MC leading field, and the Dst index. We found that 62% (39/63) of the events with the sigmoids generated geomagnetic storms ($Dst \leq -50$). In our original data set of 133 events, 70 had no clear sigmoids. Of these events, 47% (33/70) were not followed by geomagnetic storms. This implies that the CMEs with sigmoids are more geoeffective.

[12] Under the assumption that the southward component in a CME source region is a control parameter that determines whether a geomagnetic storm will be produced, we present the results in contingency tables of the CME geoeffectiveness. Table 3 shows the distribution of geomagnetic storms by field orientation in the CME source region, determined by the CFR and FFF models. Note that the FFF model gives the inverse of the CFR: When one predicts south, the other predicts north. Therefore only two rows are needed. To obtain the contingency table, the first two columns are summed. Thus there were 28 storms following southward fields for the CFR model, and 11 for the FFF model. Figure 4 presents the statistical information from Table 3, using the definitions in Table 1. As can be seen from Figure 4 and Table 3, the prediction of geomagnetic storms based on the CFR model is much better than that on the FFF model. In the case of the CFR model, PODy (0.72) and CSI (0.56) are larger than the values (0.5 and 0.33) predicted by random prediction as well as FAR (0.3) is less than the value (0.5) by random prediction. Even though these statistical values do not imply a good prediction, it is evident that the southward field components in the CME source regions are more effective in producing geomagnetic storms than the northward field, supporting *Pevtsov and Canfield*'s [2001] results.

[13] We identified the ICME classification (MC or EJ) for 78% (49/63) of the events. Here 46% (29/63) of the events are identified as MC and 32% (20/63) of the events as EJ. In Table 4, we made contingency tables for MC, EJ and Others (those not clearly distinguishable), respectively. Figure 5 presents the statistical verification parameters from the contingency tables. As seen in the figure and the table, all statistical parameters for the MC are much better than those for the EJ. In the case of MC, PODy (0.86), CSI (0.73), and FAR (0.14) show a very good prediction, which are much better than those from Figure 4. The above facts may be explained by the magnetic structure of a MC being much better conserved through the heliosphere than that of a EJ that is usually thought to be disturbed by complex heliospheric environment such as multi-CMEs [*Burlaga et al.*, 2001; *Wang et al.*, 2002]. Moreover, the magnetic structure of an ICME (especially, MC) has been shown to come from the CME source region [*Bothmer and Schwenn*, 1994; *Yurchyshyn et al.*, 2005]. In the case of MC, we may predict well the occurrence of a geomagnetic storm according to the field orientation in a CME source region if its sigmoidal shape is well identified. In the case of EJ or Others, most of the statistical parameters are not so good.

[14] Table 5 shows a contingency table between the magnetic field direction in CME source regions and the directions of MC leading fields. It is found that for 83% (24/29) of the events, the directions of MC leading field are consistent with the field orientations in CME source regions. This result supports the idea that the field directions observed in the MC usually do not change from their origin in the CME source region; this is consistent with the results shown in Figure 5. It is also in agreement with *Song et al.* [2005] who presented a close relationship between the orientation of overlying magnetic fields in the source region and the hourly averaged ACE measurements of the Bz component of the interplanetary magnetic fields, that is believed to be the indicator of geomagnetic storms. On the other hand, we examined the IMF data for 6 storms with north-oriented magnetic clouds. Out of these events, the main phases of geomagnetic storms were overlapped with sheath regions preceding the clouds for three events and associated with both the sheath regions and the MCs themselves for other two events. Thus the above five events

Table 2. Observational Summary of 63 CME-ICME Pairs

AR Number	Eruption Date and Time[a]	Location	Sigmoidal Shape[b]	Orientation[c]	MC/EJ[d]	Leading Field[e]	*Dst* Index
8005	961219 1630	S14W09	S	N	MC	N	−18
none	970106 1510	S18E06	S	S	MC	S	−78
8027	970407 1427	S30E19	S	S	EJ	...	−82
8032	970416 0735	S22E04	S	S	MC	S	−108
8038	970512 0630	N21W08	In-S	S	MC	S	−115
8040	970521 2100	N06W13	S	S	MC	S	−74
8048	970605 2255	S25W17	S	S	MC	S	−85
8064	970730 0445	N23W21	In-S	S	MC	S	−48
8076	970830 0130	N28E11	S	N	MC	N	−98
none	970928 0108	N22E05	In-S	S	MC	N	−98
8090	971006 1528	N54E46	S	S	MC	S	−130
8100	971104 0610	S20W27	In-S	N	MC	S	−110
8156	980214 0655	S24E23	In-S	N	EJ	...	−100
8375	981104 0418	N18E07	S	N	EJ	...	−92
8375	981105 2044	N18W07	S	N	MC	N	−148
8453	990209 0533	S29W36	S	S	...	...	−16
none	990413 0330	N16E00	In-S	S	MC	S	−90
8525	990503 0606	N15E32	In-S	S	EJ	...	−18
8602	990629 0554	N18E07	S	N	...	...	−26
8602	990703 1954	N16W55	S	N	MC	N	−8
8649	990728 0906	S15E03	S	S	EJ	...	−37
8651	990731 1126	S25E29	S	N	EJ	...	−17
8651	990801 1927	N25E13	S	N	EJ	...	−7
8806	991222 0230	N10E30	S	N	EJ	...	−27
8858	000210 0230	N31E04	In-S	S	MC	S	−169
8858	000212 0431	N28W23	In-S	S	MC	S	−78
8869	000217 2006	S25W12	S	S	MC	N	−27
8976	000430 0854	S11W18	S	N	...	...	−35
9028	000602 1030	N10E23	In-S	S	...	...	−35
9026	000606 1554	N20E18	S	N	EJ	...	−87
9026	000607 1630	N23E03	In-S	S	EJ	...	−36
9052	000620 0910	S30W30	S	S	EJ	...	−34
9070	000708 2350	N18W12	In-S	S	EJ	...	−40
9077	000710 2150	N18E49	In-S	S	...	...	−58
9077	000711 1327	N18E27	In-S	S	...	...	−35
9070	000712 2030	N16W64	In-S	S	MC	N	−60
9077	000714 1054	N22W07	In-S	S	MC	S	−300
9097	000725 0330	N06W08	In-S	S	MC	S	−74
9114	000809 1630	N11W01	In-S	S	MC	S	−237
9182	001009 2350	N01W14	S	N	MC	N	−110
9213	001103 1826	N02W02	In-S	S	MC	S	−169
9350	010215 1354	N07E12	In-S	N	...	...	−20
9360	010228 1450	S02W12	S	S	EJ	...	−74
9384	010316 0350	N01W11	In-S	S	MC	S	−165
9380	010319 0526	S05W00	S	S	EJ	...	−75
9393	010325 1706	N16E25	In-S	S	EJ	...	−98
9393	010402 2206	N19W72	In-S	S	...	...	−38
9415	010409 1554	S21W04	S	S	MC	S	−270
9415	010410 0530	S23W09	S	S	MC	S	−257
9415	010411 1331	S22W27	S	S	EJ	...	−66
9434	010419 1230	N20W20	In-S	S	MC	N	−105
9433	010426 1230	N17W31	In-S	S	MC	S	−33
9448	010510 0131	N21W30	In-S	S	...	...	−46
none	010809 1030	N05W05	In-S	N	...	...	−30
9585	010827 1726	N10W30	S	N	MC	N	−40
9632	010924 1030	S12E23	S	S	...	...	−103
9636	010929 1154	N13E03	S	S	EJ	...	−182
9661	011019 1650	N15W28	S	N	EJ	...	−166
9672	011025 1526	S16W21	S	N	...	...	−160
9682	011029 1150	N12E23	S	N	EJ	...	−107
9684	011104 1635	N08W18	In-S	S	...	...	−277
9704	011117 0530	S13E42	S	N	...	...	−32
9704	011222 2330	S18W38	S	N	EJ	...	−213

[a]Dates are given as yymmdd. Time is universal time.
[b]Indicates the sigmoidal shape seen in Yohkoh SXT image. S is S-shape and In-S is inverse S-shape.
[c]Indicates the field orientation of a X-ray sigmoid based on CFR model. S is southward orientation of the magnetic field and N is northward orientation of the magnetic field in a CME source region.
[d]Indicates the ICME classification. MC indicates a magnetic cloud and EJ indicates an ejecta.
[e]Indicates the direction of MC leading field. S is southward magnetic field and N is northward magnetic field.

Table 3. Distribution of Geomagnetic Storms by Field Orientations in the CME Source Region Determined by the CFR and FFF Models

Field Orientation Model	Storm		Nonstorm,
	$Dst \leq -100$	$-100 < Dst \leq -50$	$Dst > -50$
CFR southward, FFF northward	14	14	13

may correspond to geomagnetic storms caused by shock compression. In the one exceptional event, the main phase of the storm was overlapped with the south-oriented trailing part of the MC. Thus the fraction of these events to the all storms is about 15% (6/39) and its fraction to all events under consideration is about 10% (76/63).

[15] Our results differ from *Leamon et al.* [2002] who showed that the correlation between the predicted orientation by CFR model and the observed IMF Bz component of magnetic cloud leading field was only 50% for the 46 solar eruption events. Unfortunately, they did not describe how to determine the orientation of MC leading fields. We have examined their data and independently determined their leading field directions as follows. First, we determined the starting times of MCs by using the catalogues of *Cane and Richardson* [2003] and the MC web page. When the corresponding data are not available, we independently determined the arrival times of the MCs at Earth, some 2–3 days after the solar eruptions by identifying the IMF structures according to the conventional criteria of MC identification, as already described in section 2.1. Second, we identified their leading field directions as the field orientations at the first part of sinusoidal IMF field variation. As a result, we could determined the leading field directions of the 22 MCs whose IMF rotation patterns are relatively evident and for which the IMF data are available from the ACE and/or WIND data. We found that, for a large fraction of the events (15/22), the field orientation in the CME source region is consistent with the leading edge in MC. Even though this result is different from *Leamon et al.* [2002], it is consistent with the result given in Table 5 and with those of *Song et al.* [2005]. We hope that this issue will be more clarified in the near future.

[16] For the evaluation of statistical significance of the results, we employed Fisher's exact test for a 2×2 contingency table, which is a test of the null hypothesis that the row classification factor and the column classification factor are independent. The probabilities for null hypothesis are 0.12 for Table 3, 0.13, 0.46, 0.41 for Table 4, and 0.002 for Table 5. The results are nearly marginal for MC and just statistical noises for EJ and Others. However, the contingency table of the field orientation based on CFR model versus the direction of MC leading field (Table 5) shows that the consistency between two field directions has a relatively significant statistical significance (0.998 = 1-0.002).

4. Summary and Conclusion

[17] In this study we have examined the CME geoeffectiveness characterized by Dst ≤ -50 nT according to the field orientation (whether N or S) of the CME source regions and to the ICME classification (MC or EJ). For this we considered 133 CME-ICME pairs (1996 to 2001) whose CME source locations were identified by SOHO/LASCO and SOHO/EIT data. Then, using the Yohkoh SXT data, we were able to identify the shapes (S or Inverse-S) of X-ray sigmoids associated with 63 of these CMEs. To determine the field orientation in the sigmoids, we applied the CFR model and the FFF model to these 63 sigmoids. The ICMEs were classified into MC, EJ, or Others according to the conventional criteria. Using the assumption that the southward component in a CME source region is a control parameter for the production of a geomagnetic storm, we present the contingency tables of the CME geoeffectiveness depending on the field orientation and the ICME classification. Major results from this study are as follows.

[18] 1. All statistical parameters computed from the information in the contingency tables of the solar field orientation versus the geomagnetic storm (shown in Figure 4) imply that the prediction of geomagnetic storms (Dst ≤ -50 nT) based on the CFR model is much better than that on the FFF model. This result supports those of *Pevtsov and Canfield* [2001].

[19] 2. All the statistical parameters from the contingency tables for MC and EJ (shown in Figure 5) indicate that the predictions based on MC are much better than those based on EJ, implying that the field orientation of the MC is well conserved through the heliosphere, while in the EJ it is disturbed by other heliospheric disturbances.

[20] 3. We also found that for about 86% (23/29) of the MCs, the directions of their leading fields are consistent with those in the CME source regions.

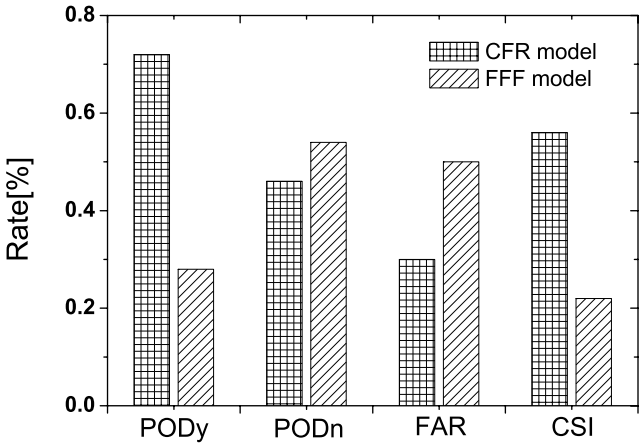

Figure 4. Statistical verification parameters from the contingency information given in Table 3.

Table 4. Contingency Tables of the Field Orientation Determined With the CFR Model, Versus Geomagnetic Storm Occurrence for the Three ICME Subgroups (MC, Ejecta, and Others)

	MC		EJ		Others[c]	
CFR Model	Storm[a]	Nonstorm[b]	Storm	Nonstorm	Storm	Nonstorm
Southward	19	3	6	5	3	5
Northward	4	3	6	3	1	5

[a]Storm: Dst ≤ -50.
[b]Nonstorm: Dst > -50.

[21] Our results confirm that the southward orientations in significant fraction of ICMEs originate from CME source regions and they play an important role in producing geomagnetic storms. Such a tendency is much stronger for MCs than for other ICMEs. Thus the identification of magnetic field direction in CME source regions is necessary for making an empirical forecast model to predict geomagnetic storms. If one knows whether a ICME will interact with other ICMEs, this information may be used to predict whether this ICME will be MC or EJ. In this regard, the monitoring of ICME propagation through the heliosphere using IPS observations [*Jackson et al.*, 2003] is expected to be helpful in improving the forecast. We also note that there are also some exceptional events (the false alarms) for the prediction based on solar southward field, as shown in Tables 3 and 4. These events may be related to other physical characteristics of CMEs or ICMEs. As already mentioned in the introduction, we are examining such possibilities [e.g., *Moon et al.*, 2005; *Kim et al.*, 2005] using an extensive sample of data from 1996 to 2003.

[22] In this study, we have only examined 63 CME- Dst pairs with the sigmoids out of 133 CME-ICME pairs from 1996–2001 since Yohkoh data were available until 2001. Thus it is noted that all statistical parameters such as success rate apply to 50% (63/133) of the CME/ICME pairs studied. As shown in the last section, the Fisher's exact test for a 2×2 contingency table shows that while the consistency between solar southward field direction and geomagnetic storms are statistically marginal for MC, the consistency between solar and MC field directions has a relatively significant statistical significance (99.8%). Therefore we hope that this issue will be more clarified using the upcoming future space missions such as Solar-B and SDO (Solar Dynamic Observatory).

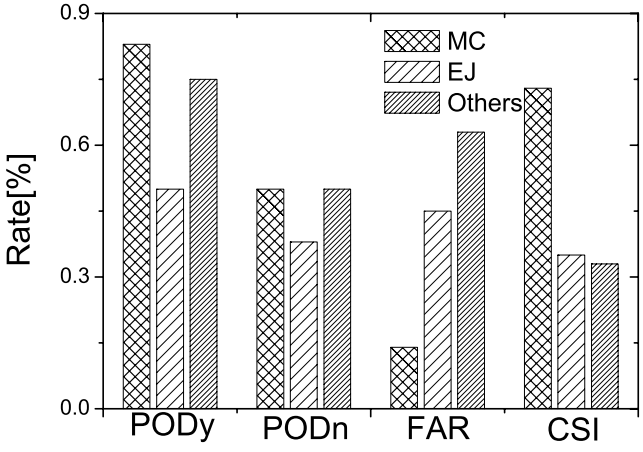

Figure 5. Statistical verification parameters from the contingency table given in Table 4.

Table 5. Contingency Table of the Field Orientation Based on CFR Model Versus the Direction of MC Leading Field

	Leading Field of MC	
CFR Model	Southward	Northward
Southward	18	4

[23] **Acknowledgments.** The authors greatly appreciate the referees' constructive comments. This work has been supported by the MOST grants (M1-0104-00-0059 and M1-0407-00-0001) and by the Korea Research Foundation (KRF-2005-070-C00059) of the Korean Government. The CME catalog we have used is generated and maintained by the Center for Solar Physics and Space Weather, Catholic University of America, in cooperation with the Naval Research Laboratory and NASA. SOHO is a project of international cooperation between ESA and NASA. The solar wind and magnetic field data of ACE and WIND were provided by NASA's CDAWeb and Omniweb sites.

[24] Lou-Chuang Lee thanks Zdenka Smith and the other reviewer for their assistance in evaluating this paper.

References

Baek, J.-H., D.-Y. Lee, K. C. Kim, C. R. Choi, Y. D. Park, Y.-J. Moon, and K.-S. Cho (2005), A statistical analysis of solar wind dynamic pressure pulses during geomagnetic storms, *J. Astron. Space Sci.*, *22*, 419.

Bothmer, V., and D. M. Rust (1997), The field configuration of magnetic clouds and the solar cycle, in *Coronal Mass Ejections*, *Geophys. Monogr. Ser.*, vol. 99, edited by N. Crooker, J. A. Joselyn, and J. Feynman, pp. 139–146, AGU, Washington, D.C.

Bothmer, V., and R. Schwenn (1994), Eruptive prominences as sources of magnetic clouds in the solar wind, *Space Sci. Rev.*, *70*, 215.

Burlaga, L. F. (1995), *Interplanetary Magnetohydrodynamics*, Oxford Univ. Press, New York.

Burlaga, L. F., R. M. Skoug, C. W. Smith, D. F. Webb, T. H. Zurbuchen, and A. Reinard (2001), Fast ejecta during the ascending phase of solar cycle 23: ACE observations, 1998–1999, *J. Geophys. Res.*, *106*, 20,957.

Cane, H. V., and I. G. Richardson (2003), Interplanetary coronal mass ejections in the near-Earth solar wind during 1996–2002, *J. Geophys. Res.*, *108*(A4), 1156, doi:10.1029/2002JA009817.

Cho, K.-S., Y.-J. Moon, M. Dryer, C. D. Fry, Y.-D. Park, and K.-S. Kim (2003), A statistical comparision of interplanetary shock and CME propagation models, *J. Geophys. Res.*, *108*(A12), 1445, doi:10.1029/2003JA010029.

Fenrich, R. R., and J. G. Luhmann (1998), Geomagnetic reaponse to magnetic clouds of differents polarity, *Geophys. Res. Lett.*, *25*, 2999.

Fry, C. D., M. Dryer, Z. Smith, W. Sun, C. S. Deehr, and S.-I. Akasofu (2003), Forecasting solar wind structures and shock arrival times using an ensenble of model, *J. Geophys. Res.*, *108*(A2), 1070, doi:10.1029/2002JA009474.

Gopalswamy, N., A. Lara, S. Yashiro, M. L. Kaiser, and R. A. Howard (2001), Predicting the 1-AU arrival times of coronal mass ejections, *J. Geophys. Res.*, *106*, 29,207.

Gosling, J. T. (1990), Coronal mass ejections and magnetic flux ropesin interplanetary space, in *Physics of Magnetic Flux Ropes*, *Geophys. Monogr. Ser.*, vol. 58, edited by C. T. Russell, E. R. Priest, and L. C. Lee, pp. 343–364, AGU, Washington, D.C.

Jackson, B. V., P. P. Hick, and A. Buffington (2003), Time-dependent tomography of heliosheric structures using IPS and Thomson scattering observations, in Proceedings of ISCS 2003 Symposium on Solar Variability as an Input to the Earth's Environment, *ESA SP-535*, edited by A. Wilson, p. 823, Eur. Space Agency, Paris.

Kim, R.-S., K.-S. Cho, Y.-J. Moon, Y.-H. Kim, Y. Yi, M. Dryer, S.-C. Bong, and Y.-D. Park (2005), Forecast evaluation of the CME geoeffectiveness using halo CMEs from 1997 to 2003, *J. Geophys. Res.*, *110*, A11104, doi:10.1029/2005JA011218.

Leamon, R. J., R. C. Canfield, and A. A. Pevtsov (2002), Properties of magnetic clouds and geomagnetic storms associated with eruption of

coronal sigmoids, *J. Geophys. Res.*, *107*(A9), 1234, doi:10.1029/2001JA000313.

Manoharan, P. K., N. Gopalswamy, S. Yashiro, A. Lara, G. Michalek, and R. A. Howard (2004), Influence of coronal mass ejection interaction on propagation of interplanetary shocks, *J. Geophys. Res.*, *109*, A06109, doi:10.1029/2003JA010300.

McAllister, H., and S. F. Martin (2000), The essential role of magnetic reconnection in erupting prominences and CMEs, *Adv. Space Res.*, *26*, 469.

Moon, Y.-J., K.-S. Cho, M. Dryer, Y.-H. Kim, S.-C. Bong, J. Chae, and Y. D. Park (2005), New geoeffective parameters of very fast halo coronal mass ejections, *Astrophys. J.*, *624*, 414.

Pevtsov, A. A., and R. C. Canfield (2001), Solar magnetic fields and geomagnetic events, *J. Geophys. Res.*, *106*, 25,191.

Rust, D. M. (1994), Spawning and shelding helical magnetic fields in the solar atmosphere, *Geophys. Res. Lett.*, *21*, 241.

Smith, Z., M. Dryer, E. Ort, and W. Murtagh (2000), Performance of interplanetary shock prediction models: STOA and ISPM, *J. Atmos. Sol. Terr. Phys.*, *62*, 1265.

Song, H., V. B. Yurchyshyn, and H. Wang (2005), Towards real-time automated prediction of geo-magnetic storms based on observations of source regions of halo CMEs, *Eos Trans. AGU*, *8618*, Spring Meet Suppl., Abstract SP23A-01.

Wang, Y. M., P. Z. Ye, S. Wang, G. P. Zhou, and J. X. Wang (2002), A statistical study on the geoeffectiveness of Earth-directed coronal mass ejections from March 1997 to December 2000, *J. Geophys. Res.*, *107*(A11), 1340, doi:10.1029/2002JA009244.

Wu, C. C., and R. P. Lepping (2002a), Effects of magnetic clouds on the occurance of geomagnetic storms: The first 4 years of Wind, *J. Geophys. Res.*, *107*(A10), 1314, doi:10.1029/2001JA000161.

Wu, C. C., and R. P. Lepping (2002b), Effect of solar wind velocity on magnetic cloud-associated magnetic storm intensity, *J. Geophys. Res.*, *107*(A11), 1346, doi:10.1029/2002JA009396.

Yurchyshyn, V. B., H. Wang, P. R. Goode, and Y. Deug (2001), Orientation of the magnetic fields in interplanetary flux ropes and solar filaments, *Astrophys. J.*, *563*, 381.

Yurchyshyn, V. B., H. Wang, and V. Abramenko (2003), How directions and helicity of erupted solar magnetic fields define geoeffectiveness of coronal mass ejections, *Adv. Space Res.*, *32*, 10.

Yurchyshyn, V. B., H. Wang, and V. Abramenko (2004), Correlation between speeds of coronal mass ejections and the intensity of geomagnetic storms, *Space Weather*, *2*, S02001, doi:10.1029/2003SW000020.

Yurchyshyn, V., Q. Hu, and V. Abramenko (2005), Structure of magnetic fields in NOAA active regions 0486 and 0501 and in the associated interplanetary ejecta, *Space Weather*, *3*, S08C02, doi:10.1029/2004SW000124.

Zhang, G., and L. F. Burlaga (1988), Magnetic clouds, geomagnetic disturbances, and cosmic ray decreases, *J. Geophys. Res.*, *93*, 2511.

J.-H. Baek, K.-S. Cho, Y.-H. Kim, Y.-J. Moon, and Y. D. Park, Korea Astronomy and Space Science Institute, Daejon, South Korea. (yjmoon@kasi.re.kr)

H.-Y. Chang and S. M. Kang, Department of Astronomy and Atmospheric Sciences, Kyungpook National University, Daegu, South Korea.